AJNR

Quantitative Characterization of the Corticospinal Tract at 3T

D.S. Reich, S.A. Smith, C.K. Jones, K.M. Zackowski, P.C. van Zijl, P.A. Calabresi and S. Mori

AJNR Am J Neuroradiol 2006, 27 (10) 2168-2178
http://www.ajnr.org/content/27/10/2168

ORIGINAL RESEARCH

Quantitative Characterization of the Corticospinal Tract at 3T

D.S. Reich
S.A. Smith
C.K. Jones
K.M. Zackowski
P.C. van Zijl
P.A. Calabresi
S. Mori

BACKGROUND AND PURPOSE: White matter tract–specific imaging will probably become a major component of clinical neuroradiology. Fiber tracking with diffusion tensor imaging (DTI) is widely used, but variability is substantial. This article reports the ranges of MR imaging appearance and right-left asymmetry of healthy corticospinal tracts (CST) reconstructed with DTI.

METHODS: For 20 healthy volunteers, whole-brain DTI data were coregistered with maps of absolute T1 and T2 relaxation times and magnetization transfer ratio (MTR), all acquired at 3T. For each individual, the 2 reconstructed CSTs and their asymmetry were analyzed with respect to the number of fibers reconstructed; tract volume; and individual MR imaging parameters restricted to the tracts. Interscan variability was estimated by repeat imaging of 8 individuals.

RESULTS: Reconstructed fiber number and tract volume are highly variable, rendering them insensitive to abnormalities in disease. Individual tract-restricted MR imaging parameters are more constrained, and their population averages and normal ranges are reported. The average population asymmetry is generally zero; therefore, normal ranges for an index of asymmetry are reported. By way of example, CST-restricted MR imaging parameters and their asymmetries are shown to be abnormal in an individual with multiple sclerosis who had a lesion affecting the CST.

CONCLUSIONS: The results constitute a normative dataset for the following imaging parameters of the CST: T1, T2, MTR, fractional anisotropy, mean diffusivity, transverse diffusivity, and the 3 diffusion tensor eigenvalues. These data can be used to identify, characterize, and establish the significance of changes in diseases that affect the CST.

Fiber tracking with diffusion tensor imaging (DTI)[1,2] is likely to emerge as a powerful clinical tool for assessing pathway-specific abnormalities in neurologic disease. Because many brain functions—including sensation, locomotion, and some aspects of cognition—involve specific white matter tracts, the ability to assess tract-specific damage with MR imaging may allow tighter correlations between disability and imaging abnormalities. This, in turn, may enable more specific diagnosis and prognostication, as well as objective evaluation of the effects of emerging therapies.

Unfortunately, the variability in current tract reconstruction techniques renders accurate detection of abnormalities difficult. This variability is due to limitations in the resolution of DTI, even at high magnetic fields, and to the iterative nature of the tract reconstruction algorithms, in which errors accumulate and become amplified.[3-6] Accurate quantification of the variability—essentially, the range of results among healthy individuals—would reduce the chance of drawing spurious conclusions from DTI studies.

Received October 16, 2005; accepted after revision January 25, 2006.

From the Departments of Neurology (D.S.R., S.A.S., P.A.C.), Radiology (D.S.R., S.A.S., C.K.J., P.C.v.Z., S.M.), Biophysics (S.A.S., P.C.v.Z.), and Physical Medicine and Rehabilitation (K.M.Z.), Johns Hopkins University, Baltimore, Md; and the F.M. Kirby Research Center for Functional Brain Imaging (S.A.S., C.K.J., P.C.v.Z., S.M.) and the Department of Physical Medicine and Rehabilitation (K.M.Z.), Kennedy Krieger Institute, Baltimore, MD.

This work was supported by grants NIH RR15241, AG20012, and EB000991 (S.A.S., C.K.J., P.C.v.Z, S.M.), the National Multiple Sclerosis Society, The Nancy Davis Center Without Walls (P.A.C., D.S.R.), and Philips Medical Systems (C.K.J.).

Dr. van Zijl is a paid lecturer for Philips Medical Systems, an arrangement that has been approved by Johns Hopkins University in accordance with its conflict-of-interest policies.

Presented in part at: Annual Meetings of the American Society of Neuroradiology, Toronto, Canada, May 21–27, 2005; American Academy of Neurology, Miami Beach, Fla, April 9–16, 2005; and International Society of Magnetic Resonance in Medicine, Miami Beach, Fla, May 7–13, 2005.

Please address correspondence to Daniel S. Reich, MD, PhD, 600 N Wolfe St, Pathology 509, Baltimore, MD 21287; e-mail: dreich2@jhmi.edu

In this study, we focus on the variability in parameters derived from reconstructed corticospinal tracts (CSTs) in the brain and also on quantifying the range of asymmetry between the right and left CSTs in healthy volunteers. In general, in diseases that present asymmetrically, including multiple sclerosis (MS), stroke, and many tumors, the asymmetry between involved tracts is expected to be greater than that in controls. This is intuitively true at the level of a lesion; in MS, for example, the ipsilateral tract has a prolonged T2 relaxation time as it passes through a plaque. However, long-range effects of lesions along the affected tracts, such as wallerian degeneration or dying-back axonopathy,[7-9] might also increase the asymmetry between tracts, which might therefore serve as a sensitive marker of clinically relevant tract-specific abnormalities. If the quantitative detection of asymmetry is sufficiently sensitive, it might even detect abnormalities not recognized on standard imaging techniques.

Our assessment of the CST is based on the results of MR imaging at 3T and focuses on reconstructed tracts as opposed to specific regions of interest within the tracts. Because some conditions preferentially affect different regions of the brain and to limit variability caused by tracking over long distances, we performed 3 separate tract reconstructions: the whole-brain portion (extending from the cerebral cortex to the medulla), the hemispheric (supratentorial) portion, and the brain stem portion.

For each reconstruction, we examined the right and left tracts for the number of fibers and total volume (related but not identical quantities) and also for various quantitative parameters derived from the MR imaging maps restricted to the tracts. These include parameters derived from the DTI data, including fractional anisotropy (FA, thought to reflect the degree to which axons at a given location tend to run together) and mean diffusivity (MD, a measure of the rate of diffusion of water within tissue). They also include parameters derived from additional coregistered MR images: specifically, T1 re-

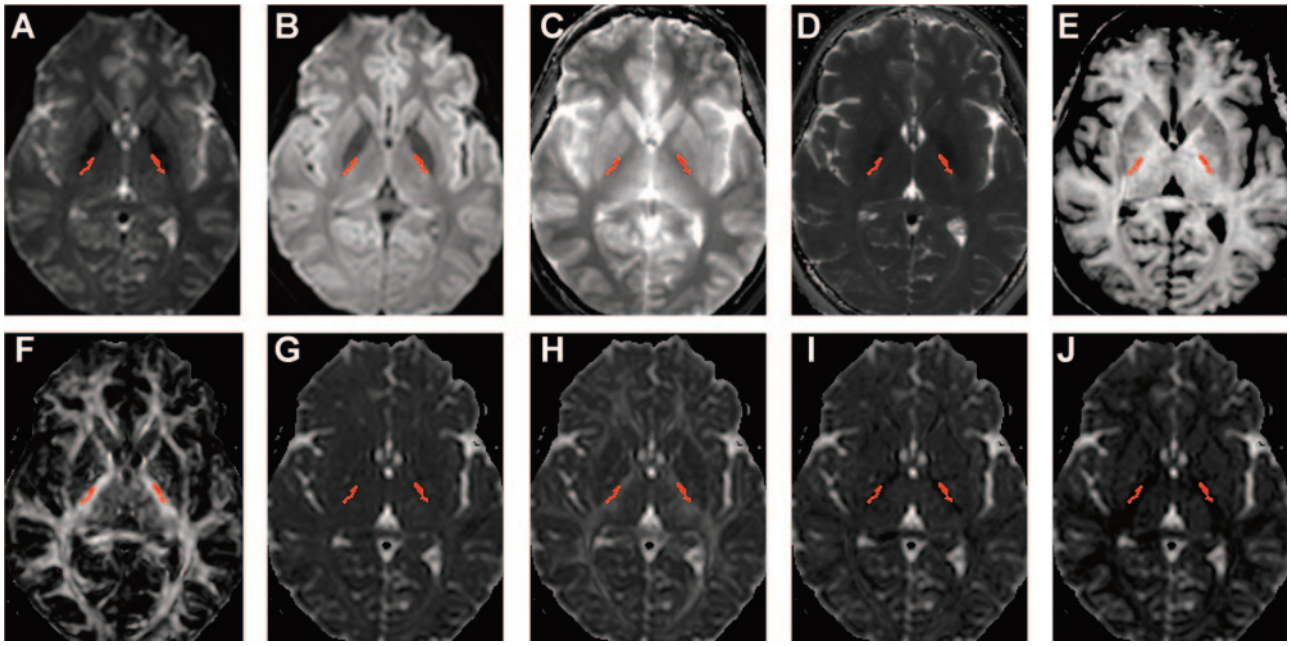

Fig 1. Corticospinal tracts of a 32-year-old healthy woman. In these axial sections at the level of the internal capsule, voxels containing the CSTs reconstructed by the whole-brain method are rendered in red. *A*, Minimally diffusion-weighted map. *B*, Mean diffusion-weighted map. *C*, Absolute T1. *D*, Absolute T2. *E*, MTR. *F*, FA. *G*, MD. *H*, λ_1; *I*, λ_2; *J*, λ_3. The map of transverse diffusivity, $\lambda_\perp$, is not shown.

laxation time, T2 relaxation time, and magnetization transfer ratio (MTR). These scans frequently show abnormalities in neurologic disorders. MTR, in particular, is a sensitive and early indicator of disease activity in MS,[10] and T1 within the CST is correlated with motor disability.[11]

To illustrate the utility of this technique, we present results from a single individual with relapsing-remitting MS who had damage to 1 CST, causing hemiparesis. This individual had abnormal MR imaging parameters within the CST as well as abnormal asymmetry between the 2 CSTs.

Methods

MR Imaging. We acquired data on 20 healthy volunteers (median age at time of first scanning, 31 years; range, 21–55 years; 15 women and 5 men). We repeated the scans on 8 of these individuals 2–4 times, separated by intervals of up to 14 months. Scanning was performed on an Intera 3T scanner (Philips Medical Systems, Best, the Netherlands) and covered the whole brain. All datasets were reconstructed to 0.83-mm in-plane resolution and 60 axial 2.2-mm sections, and many were acquired at this resolution as well. Imaging protocols were approved by the local institutional review boards, and informed consent was obtained.

We obtained DTI data from all individuals. Scanning details were as follows: single-shot spin-echo echo-planar sequence; quadrature body coil for transmission; 8-element phased-array head coil configured as a 6-element coil for reception; Sensitivity Encoding (SENSE) reduction factor, 2.5; TR $\approx$ 5 s; TE $\approx$ 65 ms; acquired resolution, 2.2 mm isotropic; 32 non-coplanar gradient directions with $b \approx 700$ s/mm^2; 1 minimally diffusion-weighted scan with $b \approx 33$ s/mm^2; 2 repetitions.[12] Scanning time per acquisition was approximately 3.5 minutes.

Off-line, we coregistered all diffusion-weighted images to the minimally diffusion-weighted acquisition by using automatic image registration (AIR) with a 6-parameter rigid-body transformation model.[13] To account for changes in section angulation due to the coregistration, we transformed each diffusion direction in the diffusion gradient table by the rotation matrix calculated by AIR. The diffusion tensor was calculated,[14] and maps of the following parameters were created (Fig 1): FA[15]; the eigenvalues of the diffusion tensor λ_1, λ_2, and λ_3; MD (the average of the 3 eigenvalues); and transverse diffusivity $\lambda_\perp$ (the average of λ_2 and λ_3). Color-coded maps were derived from the principal eigenvector weighted by FA.[16] These analyses were performed in DTI-Studio,[17] as well as with custom software written in Matlab (The Mathworks, Natick, Mass).

In 11 individuals (11 scans), we acquired multishot 3D spoiled gradient-echo echo-planar images for the estimation of absolute tissue T1 (TR, 100 ms; TE, 10 ms; flip angles $\alpha_1 = 15°$ and $\alpha_2 = 60°$; acquired resolution, 0.83 × 0.83 × 2.2 mm). The 2 scans were coregistered to one another by using AIR, and then the absolute T1 was estimated as follows:

$$T1 = \frac{-TR}{\log\left(\frac{\sin(\alpha_2) - R\sin(\alpha_1)}{\cos(\alpha_1)\sin(\alpha_2) - R\cos(\alpha_2)\sin(\alpha_1)}\right)}$$

where $R = S_{\alpha 1}/S_{\alpha 2}$, the ratio of signal intensities at the 2 flip angles.[18] Absolute T1 maps were then coregistered to the minimally diffusion-weighted image.

In 17 individuals (21 scans), we acquired multisection double-echo spin-echo images (TR, 4158 ms; TE, 28.2 and 80 ms; acquired resolution, 1.1 × 1.1 × 2.2 mm) to visualize proton-density and T2-weighted maps. Maps of absolute T2 (Fig 1) were generated by:

$$T2 = \Delta TE \ln\left(\frac{S_2}{S_1}\right)$$

where S_i is the signal intensity for echo i. We then used AIR to coregister the absolute T2 maps to the minimally diffusion-weighted map via a rigid-body nondeformable transformation model.

In 15 individuals (17 scans), we acquired MT-weighted images for the calculation of MTR (3D spoiled gradient-echo with multishot echo-planar readout; TR, 65 ms; TE, 15 ms; acquired resolution,

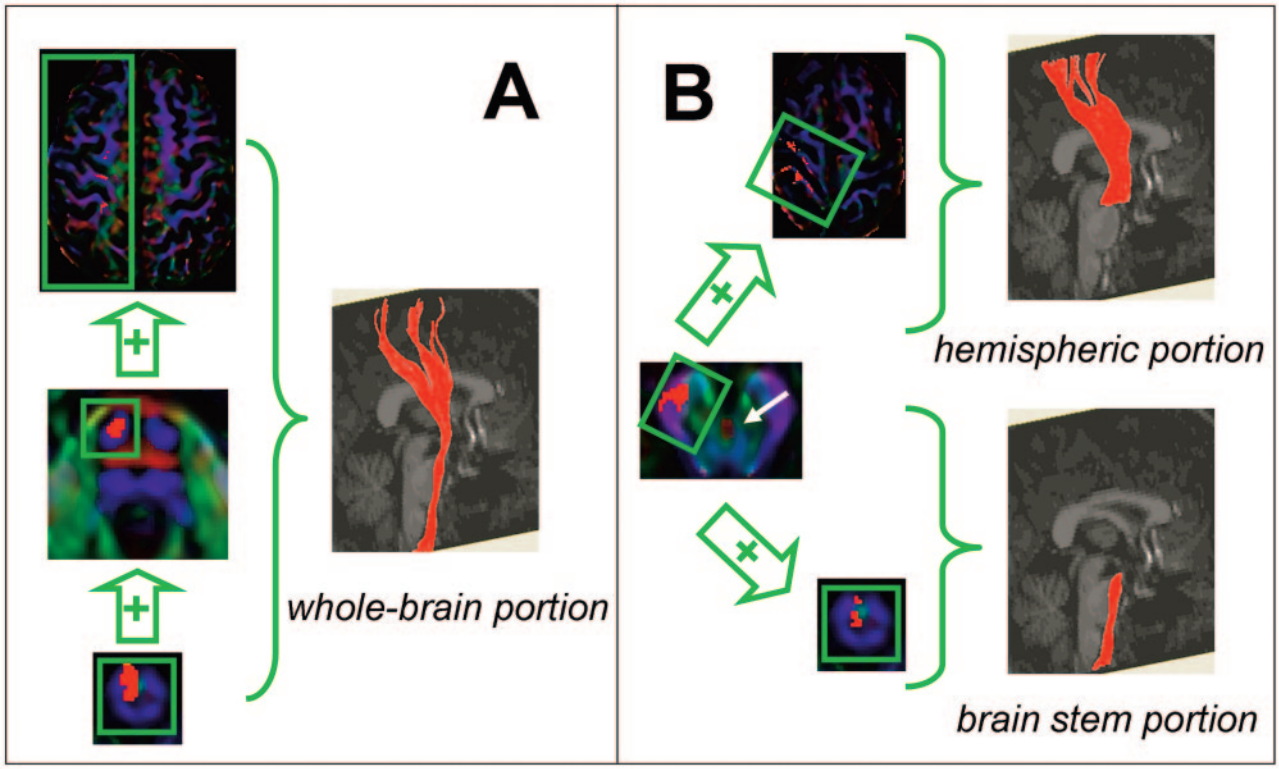

Fig 2. Right-sided corticospinal tracts, reconstructed from DTI data with ROIs chosen as described in "Methods." Axial sections are portions of color-coded maps derived from FA and the principal eigenvector. In these maps, blue represents tracts running in the rostrocaudal axis; green, anteroposterior; and red, mediolateral; oblique angles are represented by a mixture of colors. The decussation of the superior cerebellar peduncle is denoted by the white arrow at the level of the midbrain in *B*. 3D representation of the CSTs are superimposed on coregistered magnetization-prepared rapid gradient-echo scans, which are heavily T1-weighted. *A*, Reconstruction of the right whole-brain CST, with ROIs depicted in green. *B*, Reconstruction of hemispheric and brain stem portions of the right CST.

1.5 × 1.5 × 2.2 mm; 3 repetitions).[19] Scans were acquired with (S_+) and without (S_-) a 1.5-kHz off-resonance SincGauss–shaped radiofrequency saturation pulse. We coregistered the first S_- map to the minimally diffusion-weighted map and then coregistered the remaining MT-weighted maps to the coregistered S_-. From these, we calculated MTR = 1 -$<S_+>$/$<S_->$ (Fig 1).

Fiber Tracking. We used the DTI datasets to obtain 3D reconstruction of the CSTs. Fiber tracking was performed with the fiber assignment by continuous tractography (FACT) method,[1,2] implemented in DTI-Studio by a single investigator (D.S.R.). This method has been described and used extensively, and we will not cover it in detail here. Briefly, every voxel in the brain is used as a seed point for fiber tracking. For each voxel, a vector is propagated in the direction of the principal eigenvector of the diffusion tensor, and the process is repeated iteratively. Tracking stops at predefined thresholds of FA and turning angle to limit the detection of spurious fibers. We chose an FA cutoff of 0.13 and a turning angle threshold of 40°.

The procedure we used to reconstruct the trajectory of the CSTs is shown in Fig 2. We obtained 3 separate reconstructions of the 2 CSTs, covering 1) the whole-brain portion of the tract from the cortex to the medulla, 2) the hemispheric portion from the cortex to the cerebral peduncles, and 3) the brain stem portion from the cerebral peduncles to the medulla. Note that each reconstructed fiber contains a variable number of axons, so that the total number of fibers is not the same as the total number of axons. Datasets in which fewer than 5 fibers were reconstructed on either side were not further analyzed ($n = 1$ for the whole-brain reconstruction).

To reconstruct the whole-brain CST (method 1), we selected 3 primary regions of interest (ROIs) on axial sections: 1) the entire brain stem at the lowest level of the medulla included in the scan; 2) the bundle of fibers that runs predominantly in the rostrocaudal axis in the ipsilateral anterior pons, as seen on the DTI color maps; and 3) the entire ipsilateral hemisphere at the level of the central sulcus. We included all reconstructed fibers that passed between these 3 ROIs without truncation at the level of ROIs 1 and 3. If necessary, we then excluded, by hand, fibers that did not pass within the main body of the reconstructed tract. This approach identified the most robust fibers of the CST that could be tracked over the whole brain.

For the hemispheric CST (method 2), we selected 2 primary ROIs on axial sections: 1) the cerebral peduncle at the level of the decussation of the superior cerebellar peduncle and 2) the ipsilateral pre- and postcentral gyri. We included all reconstructed fibers that passed through both ROIs, truncating the fibers at the 2 ROIs, and excluded fibers that fell outside the main body of the tract. We followed a similar procedure for the brain stem CST (method 3), except that the second ROI was placed in the anterior medulla, also on an axial section. Because tracts reconstructed separately in the brain stem and hemispheres are required to traverse shorter distances, they generally contain more fibers than reconstructed whole-brain tracts.

MR Imaging Parameters. Restricted to the reconstructed CSTs, we analyzed FA, MD, the 3 tensor eigenvalues λ_1, λ_2, and λ_3, and the average of the 2 smallest eigenvalues $\lambda_\perp$; all of these parameters are derived from the DTI acquisitions. We also analyzed absolute T1, absolute T2, and MTR. Because any voxel can contribute to more than 1 fiber, we weighted the contribution of each voxel to the overall distribution of MR imaging parameters by the number of fibers that traversed it.

Asymmetry Analysis. An asymmetry index (A) quantifies the differences between the right and left CSTs:

$$A = \frac{p_R - p_L}{p_R + p_L}$$

where p_R is the statistic of interest (for example, median FA or interquartile range [IQR] of MTR) derived from the right CST and p_L, the corresponding statistic from the left CST. A can range from −1 (maximal asymmetry with the statistic on the right equal to 0) to 1 (maximal asymmetry with the statistic on the left equal to 0); $A = 0$ corresponds to equality between the statistics on the 2 sides.

Results

Typical Results from a Healthy Individual. Fig 1 shows imaging results from a 32-year-old healthy woman whose data are typical of our population; data from this individual are also used in Fig 2 to illustrate the tract identification procedure. For this individual, we reconstructed 132 fibers (with a total volume of 2.9 mL) in the right whole-brain CST; 713 fibers (4.3 mL) in the right hemispheric CST; 542 fibers (0.9 mL) in the right brain stem CST; 310 fibers (5.0 mL) in the left whole-brain CST; 1260 fibers (4.1 mL) in the left hemispheric CST; and 546 fibers (0.9 mL) in the left brain stem CST. Note that multiple fibers that have separate origins may converge along their course, so that twice the number of fibers does not necessarily correspond to twice the volume (number of voxels) subsumed.

In Fig 3, for the same individual, we show the distributions of MR imaging parameters along the CSTs and their dependence on position along the tract. The patterns displayed here are similar across individuals (not shown). For example, there is a reliable drop in FA, seen here at approximately 105 mm, which occurs as the CST fans out from the internal capsule on its trajectory toward the precentral gyrus. This feature is caused by a relative drop in the axial diffusivity, λ_1, and a concomitant increase in the transverse diffusivity, $\lambda_\perp$. Note that, for most parameters, the IQR (right column) is highest at the rostral and caudal ends of the tracts, which correspond to the areas of highest variability in tract reconstruction.

MR Imaging Parameters Across the Population. Fig 4 shows the cross-individual distributions of parameter medians and IQRs, together with 99% normal ranges derived from Gaussian distributions with the same mean and variance as the sample data. These values are summarized in Tables 1 and 2. The Gaussian assumption is justified by the Lilliefors Test for Normality[20]: for all cross-individual parameter medians and IQRs derived from the whole-brain CSTs, the null hypothesis that the underlying distributions are Gaussian cannot be rejected at $P < .01$; the only exceptions are the IQR of T2 and MTR. As illustrated in this article in a single case of MS, these cutoffs can be used to identify quantitative tract-specific abnormalities affecting the MR imaging parameters studied here.

Asymmetry. From the median and IQR of each distribution of MR imaging parameters and from the total fiber number and tract volume, we calculated asymmetry indices, referred to hereafter simply as asymmetries. As described in "Methods," the asymmetries reflect the differences between the right and left CST for each parameter. Positive asymmetries indicate that the parameter in question is larger on the right side. Asymmetries can range from −1 to 1.

In general, asymmetries in median MR imaging parameters are small in both the hemispheres (median absolute value of asymmetry indices across individuals and MR parameters, 0.012) and the brain stem (0.019), but the brain stem values are significantly larger ($P < .001$, Wilcoxon signed rank test). Asymmetries in IQR tend to be larger but still relatively small compared with asymmetries in fiber number and tract volume.

For nearly all parameters, the 99% confidence intervals of the cross-individual mean asymmetries overlap 0, indicating that these parameters are not consistently larger on one side or the other across the population. The few exceptions are as follows: for the whole-brain CST, median MD and λ_1 (both greater on the left), and IQR of T1 (greater on the right); and for the hemispheric CST, median MD and λ_3 (both greater on the left), and IQR of T1 (greater on the right). In all these cases, the median asymmetries are still small. We therefore assume that there is no bias toward one side or the other across the population and take the cross-individual mean asymmetry to be zero for all parameters. The distributions of asymmetries across individuals are well modeled by Gaussians (Lilliefors Test for Normality, $P > .01$ for all parameters), so the 99% normal ranges given in Fig 5 and Table 3 are derived from Gaussians with mean 0 and variance equal to the population sample variance.

Variability. The large asymmetry in fiber number and tract volume reflects the uncertainty inherent in the fiber tractography technique.[4,5] To quantify this uncertainty, we scanned 8 of our individuals on multiple (2–4) occasions and calculated the SD of asymmetries across those individuals. In the hemispheres, the median SD was 0.12 (range, 0.038–0.46) for fiber number and 0.091 (0.0083–0.40) for tract volume; but only 0.0081 (1.6×10^{-4}–0.043) across all median MR imaging parameters.

One useful way of displaying these data is presented in Fig 6. The advantage of plots of this type is that both the raw summary statistics and their associated asymmetries can be readily appreciated. On these plots, asymmetry is related to the distance from the central diagonal line, with positive asymmetries lying below (right > left) and negative asymmetries lying above. For most parameters, the error bars cross the line of equality, suggesting that apparent asymmetry is related to variability rather than to a true right-left difference. The least variable parameter is MTR, for which the error bars are similar in size to the data points themselves (and therefore barely visible on the graphs) for both individuals scanned more than once. Again, the scatter about the diagonal is much greater for fiber number and tract volume than for the individual MR imaging parameters, corresponding to the greater variability of these statistics.

Example: MS. Data from a single scan of an individual with relapsing-remitting MS are presented in red in Figs 4 and 5. This scan was obtained 1 year after a relapse that caused right hemiparesis, related to a gadolinium-enhancing lesion in the left centrum semiovale (not shown). The hemiparesis had largely resolved by the time of the scanning. For this individual, many of the MR imaging parameters examined, though not fiber number or tract volume, fell outside the normal range, indicating that the lesion altered the MR imaging characteristics of the affected CST. The parameters most strongly affected were hemispheric and whole-brain MD (increased), as well as hemispheric MTR (decreased), T1 (increased), and λ_1 (increased). Transverse diffusivity, $\lambda_\perp$, was also increased in the hemispheres. These changes are in the appropriate direction for MS lesions.[21] There were no definite abnormalities in the brain stem parameters for this CST.

The IQR appears to be more sensitive than the median for

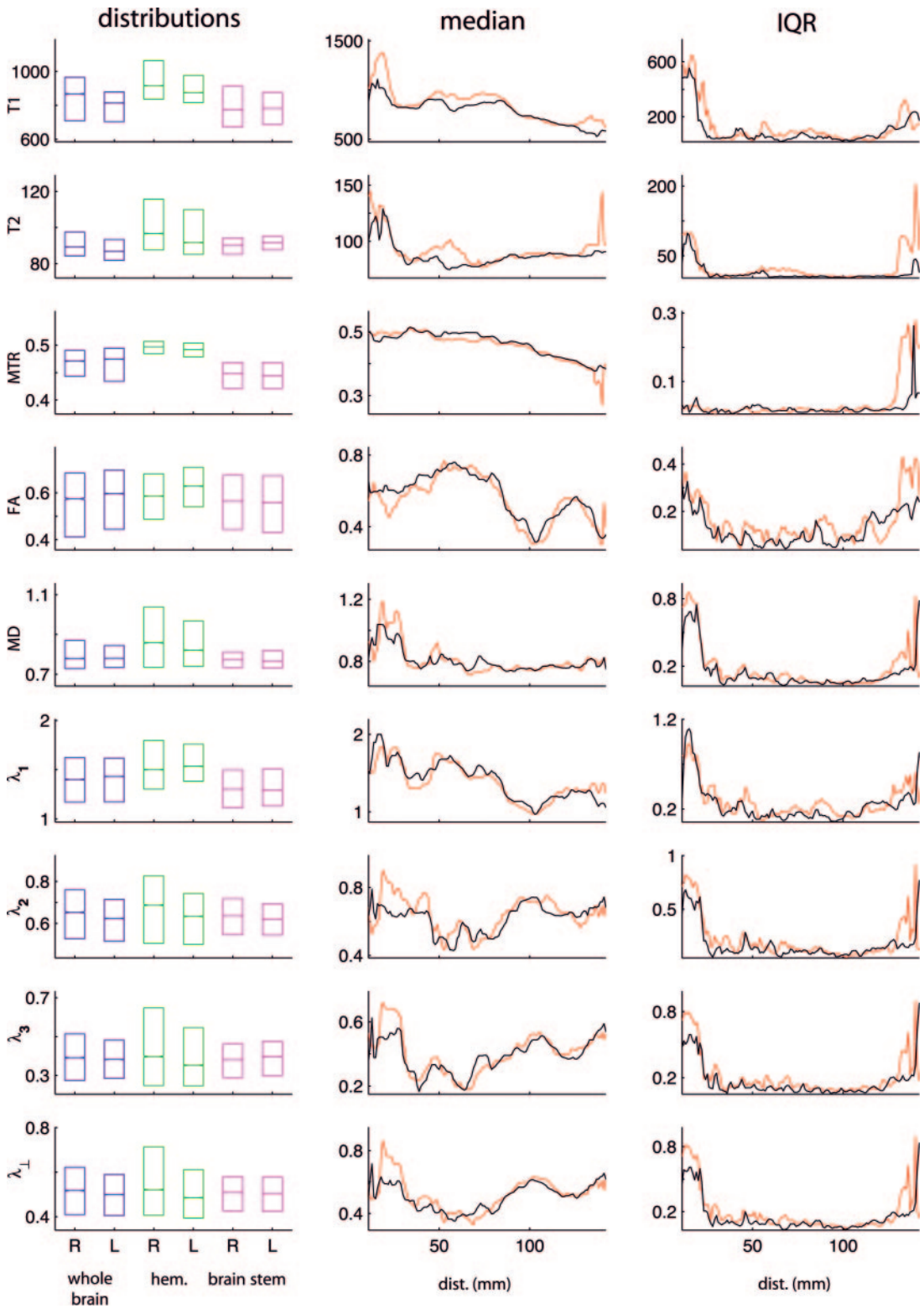

Fig 3. MR imaging parameters restricted to the corticospinal tracts of the subject shown in Figs 1 and 2. Left column shows parameter distributions restricted to the CSTs in the whole brain (blue), brain stem (green), and hemispheres (magenta). Each box shows the IQR across the entire reconstructed tract of the parameter labeled on the vertical axis, with the central line representing the median. Middle column shows median MR imaging parameters for the right (black) and left (red) CST, as a function of distance from the lowest section in the medulla. Data are taken from the whole-brain reconstructions. Right column shows IQR versus distance. For this individual, distances <20 mm correspond approximately to the medulla; 20–45 mm, to the pons; 45–60 mm, to the midbrain; 60–85 mm, to the internal capsule; 85–120 mm, to the corona radiata; and >120 mm to the subcortical white matter. For easier visualization, plots in the middle and right columns exclude highly variable data from the lowest and highest sections. Units: ms (T1, T2); 10^{-3} mm^2/s (MD, λ_1, λ_2, λ_3, $\lambda_\perp$).

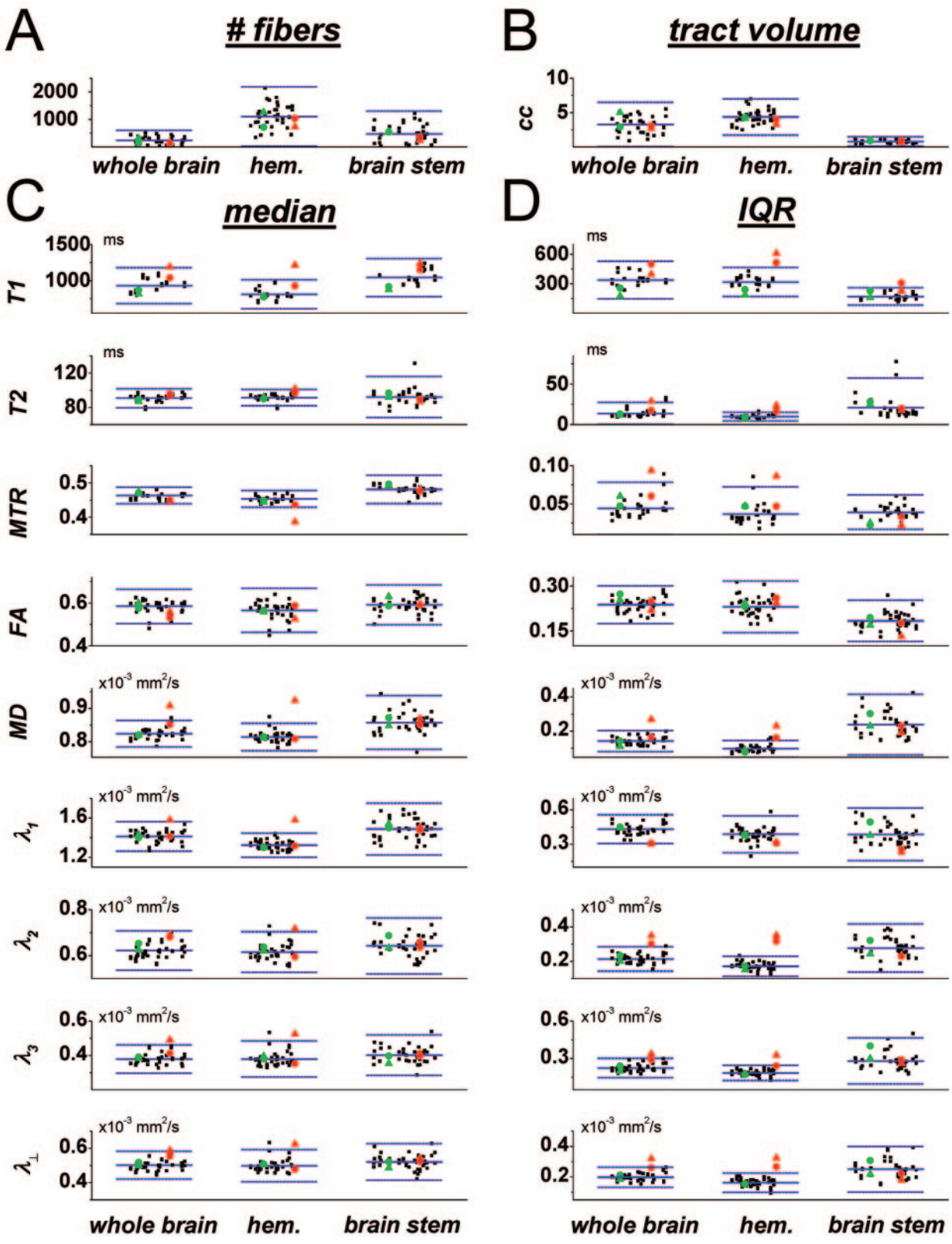

Fig 4. Properties of the reconstructed corticospinal tracts. *A*, Number of reconstructed fibers. *B*, Tract volume. *C* and *D*, Medians (*C*) and IQRs (*D*), of individual MR imaging parameters restricted to the CSTs. Black points denote healthy individuals; green, the particular healthy subject of Figs 1–3; and red, an individual with MS. For green and red points, circles denote the right CST, and triangles, the left CST; for black points, the right and left sides are not distinguished. Also shown are means (central horizontal lines) and 99% normal ranges (delimited by flanking horizontal lines) across the population of healthy individuals. Parameter type is given in the vertical axis label for each graph in *C*; the same labels apply to panel *D*. Data are randomly scattered along the horizontal axis within each category, for easier visualization. For individuals scanned more than once, cross-scan means are plotted.

Table 1: Population means and 99% normal ranges (in parentheses) of fiber number, tract volume, and MR parameter medians across our population of healthy individuals. Data obtained at 3T.

Reconstruction Type	No. of fibers	Vol. (cm^2)	T1 (ms)	T2 (ms)	MTR	FA	MD ($\times 10^4$ mm^2/s)	λ_1 ($\times 10^4$ mm^2/s)	λ_2 ($\times 10^4$ mm^2/s)	λ_3 ($\times 10^4$ mm^2/s)	$\lambda_\perp$ ($\times 10^4$ mm^2/s)
No. of individuals	*20*	*20*	*11*	*17*	*15*	*20*	*20*	*20*	*20*	*20*	*20*
Whole brain	240 (−120, 610)	3.3 (0.039, 6.5)	930 (680, 1180)	91 (80, 102)	0.46 (0.44, 0.49)	0.58 (0.51, 0.66)	7.9 (7.3, 8.5)	14 (13, 16)	6.2 (5.4, 7.1)	3.8 (3.0, 4.6)	5.0 (4.2, 5.8)
Hemispheres	1100 (28, 2200)	4.4 (1.7, 7.0)	810 (610, 1000)	92 (82, 101)	0.45 (0.43, 0.48)	0.57 (0.46, 0.67)	7.7 (7.1, 8.3)	13 (12, 15)	6.2 (5.3, 7.0)	3.8 (2.7, 4.8)	5.0 (4.1, 5.9)
Brain stem	470 (−350, 1300)	0.81 (0.14, 1.5)	1040 (780, 1300)	92 (68, 116)	0.48 (0.44, 0.52)	0.59 (0.50, 0.68)	8.4 (7.2, 9.6)	15 (12, 18)	6.4 (5.2, 7.6)	4.0 (2.8, 5.2)	5.2 (4.1, 6.3)

Note:—MTR indicates magnetization transfer ratio; FA, fractional anisotropy; MD, mean diffusivity; $\lambda_\perp$, transverse diffusivity (average of λ_2 and λ_3).

detecting MR imaging abnormalities in this individual. For example, parameters for which the median is marginally abnormal, such as hemispheric T2 and $\lambda_\perp$, have IQRs that are even further outside the normal range. In some cases, such as whole-brain MTR, the IQR is abnormal even when the median is entirely normal, though the reverse may also be true (eg, λ_1 in the whole brain and hemispheres).

Figure 5 shows that the asymmetry indices are significantly abnormal in the individual with MS for median T1, MTR, MD, and all DTI eigenvalues in the hemispheres. IQR asymmetries are abnormal for T2 and MTR. For this individual, therefore, analysis of asymmetry does not provide substantial additional information beyond analysis of raw MR imaging parameters.

We found no significant association of any of the MR imaging parameters with handedness (Fisher exact test, data not shown).

Discussion

In this article, we present the distributions of various MR imaging parameters within the CSTs reconstructed from 3T DTI data obtained from healthy volunteers. The parameters we examine are FA; MD; the 3 DTI eigenvalues λ_1, λ_2, and λ_3; transverse diffusivity $\lambda_\perp$; absolute T1; absolute T2; and MTR. For each parameter, we also present the range of asymmetry between the right and left CSTs, assessed from summary statistics (median and IQR) derived from the within-tract distributions of the MR imaging parameters. Although we have chosen to focus on the CST because it is easily reconstructed and has a well-defined function, the methods we have applied can be readily used with tracts other than the CST, both in the brain and spinal cord, and even in peripheral nerve.[22]

Technical Considerations. Although our approach can be automated and used on data from any DTI experiment, the quantitative results in Tables 1–3 may require modification for use with other equipment and scanning parameters. In principle, if absolute diffusion constants of pure tissues were measured under noiseless conditions and with infinitesimal resolution, these parameters would not matter. In practice, because we work under conditions of limited resolution, the presence of partial volume effects between tissues means that changing the resolution of the acquisition may affect the results.[23] A similar argument holds for real-world signal intensity to noise, which should be increased at higher field strengths, thereby reducing variability. This is particularly true for MTR[19] but also affects T1 and T2. Qualitatively, our results are unlikely to change significantly, and we have indeed observed similar findings in DTI data recorded with different imaging parameters on a 1.5T scanner (not shown). Moreover, it is likely that individuals with neurologic diseases that cause marked parameter abnormalities and asymmetry between the right and left tracts, as illustrated by the case of the individual with MS described here, will be readily apparent even without such precise scanner- and sequence-specific calibration.

The issue of individual DTI eigenvalues deserves special mention. Because the eigenvectors corresponding to these eigenvalues only approximate axonal geometry, a simple interpretation of the meaning of the individual eigenvalues is misleading. For this reason, most investigators have focused on MD—the average of the 3 DTI eigenvalues—because it is rotationally invariant and, therefore, easy to compare across individuals. Some investigators have examined the properties of the individual eigenvalues on the theory that λ_1 corresponds

Table 2: Population means and 99% normal ranges (in parentheses) of MR parameter interquartile ranges across our population of healthy individuals. Data obtained at 3T.

Reconstruction Type	T1 (ms)	T2 (ms)	MTR	FA	MD ($\times 10^4$ mm^2/s)	λ_1 ($\times 10^4$ mm^2/s)	λ_2 ($\times 10^4$ mm^2/s)	λ_3 ($\times 10^4$ mm^2/s)	$\lambda_\perp$ ($\times 10^4$ mm^2/s)
No. of individuals	*11*	*17*	*15*	*20*	*20*	*20*	*20*	*20*	*20*
Whole brain	340 (150, 530)	14 (0.20, 27)	0.044 (0.010, 0.078)	0.24 (0.17, 0.30)	1.4 (0.79, 2.0)	4.3 (3.1, 5.6)	2.1 (1.4, 2.8)	2.2 (1.5, 3.0)	2.0 (1.3, 2.6)
Hemispheres	320 (170, 460)	9.8 (4.6, 15)	0.037 (0.0013, 0.072)	0.23 (0.14, 0.32)	0.96 (0.47, 1.4)	3.9 (2.3, 5.5)	1.7 (1.1, 2.3)	1.9 (1.2, 2.5)	1.6 (0.99, 2.3)
Brain stem	170 (82, 260)	21 (−15, 57)	0.039 (0.017, 0.062)	0.18 (0.12, 0.25)	2.4 (0.60, 4.2)	3.9 (1.6, 6.2)	2.8 (1.4, 4.2)	2.8 (0.96, 4.6)	2.5 (1.0, 4.0)

Note:—MTR indicates magnetization transfer ratio; FA, fractional anisotropy; MD, mean diffusivity; $\lambda_\perp$, transverse diffusivity (average of λ_2 and λ_3).

to axial diffusivity along the length of an axon, whereas λ_2 and λ_3 correspond to transverse diffusivity across an axon. Perhaps unexpectedly, these individual eigenvalues are consistent across individuals.[24] Finally, some investigators report the transverse diffusivity $\lambda_\perp$, equal to the average of λ_2 and λ_3, because these 2 smallest eigenvalues have similar physical interpretations (on account of the roughly cylindric shape of axons) and are often similar in magnitude.[25] Because all these quantities might be abnormal in disease, in this article, we report all of them. Note that although the individual eigenvalues are physical quantities with units of square millimeters per second and can therefore be directly compared across individuals, additional clinically relevant information might be obtained by normalizing the eigenvalues before the cross-individual comparison. In fact, FA is one such normalization.

Variability. Tract reconstruction variability has been extensively evaluated and has many sources.[3-5,26-28] Here, our approach to assessing this variability is to scan a subset of individuals on multiple occasions. Other methods of assessing variability in tract reconstruction with DTI, even those that use powerful model-free approaches such as the bootstrap,[4,5] suffer from the drawback that they require long data-collection times.

One major source of variability is the inability of current tract-reconstruction techniques to distinguish among different tracts that pass through a single voxel,[2] because of either insufficient spatial resolution or partial volume effects.[23] Because the technique is iterative, errors that occur in 1 voxel may accumulate and propagate from voxel to voxel, compounding the problem. This can lead to confusion in tract reconstruction, so that a fiber that begins as part of the CST may veer off, for example, into neighboring tracts such as the superior cerebellar peduncle or the corpus callosum. In our analysis, these improperly reconstructed fibers—including the portions that run within the main body of the CST—are eliminated by drawing exclusionary ("NOT") ROIs. This causes artificial lowering of the fiber count and tract volume, which might lead to increased apparent asymmetry primarily affecting those quantities.

A second, related problem is the inability of DTIs to resolve "crossing" from "kissing" fiber bundles within a voxel. Indeed, we have found that the bulk of the reconstructed CSTs do not appear to decussate in the medullary pyramids, as they are known anatomically to do, but rather continue to descend in the ipsilateral medulla. In reality, the CSTs are only partially crossed,[29] and the conflation of the 2 tracts that may occur at this level can affect the results unpredictably.

Third, the choice of cutoff thresholds for tract reconstruction can have a significant impact on the identification of fibers within a bundle.[27] The FACT algorithm for tract reconstruction stops when a voxel with FA lower than a predetermined threshold is reached. Our approach in this study has been to lower the FA threshold to the extent possible and to impose a greater number of anatomic constraints on tract identification. The primary reason for this choice is that these parameters—particularly FA—tend to fall in neurologic diseases, including MS,[21] and choosing a cutoff that is too high might incorrectly exclude fibers that are damaged but still present. Thus, we have chosen an FA cutoff of 0.13 for fiber tracking, which is slightly lower than the cutoffs typically used in other studies.[27,30] We balance this choice by using more than 1 ROI to constrain the trajectory of the CST and by eliminating fibers that clearly fall outside the tract.[28] In addition, we choose relatively long segments of the tract—from the cortex to the medulla for the whole-brain portion, from the cortex to the cerebral peduncle for the hemispheric portion, and from the cerebral peduncle to the medulla for the brain stem portion. Such long segments remove from the analysis portions of fibers that appropriately run within the tract for some distance but then spuriously veer off into other tracts, as described previously.

Despite these sources of variability and mostly because of our use of prior anatomic data to initiate tract reconstruction, we suspect that our approach identifies voxels that make up the core of the tract—in theory, the least variable portion—at the expense of voxels that are more questionably part of the tract. This suspicion is confirmed by visual inspection of the identified tracts, both within individual axial sections and in 3D reconstructions, which we perform for every individual studied.

Asymmetry. A previous study used diffusion-weighted imaging to demonstrate asymmetric MD in the brain, with some structures having consistently higher MD on one side or the other across a population of healthy volunteers.[31] This asymmetry was found to be more significant in gray matter structures than in white matter tracts. In addition, postmortem analysis has revealed anatomic differences between the right and left CSTs, both in the brain and spinal cord. In the medulla, for example, the CST originating from the left precentral gyrus usually decussates at a more rostral level than its counterpart on the right.[29] Morphometric evidence[32] suggests that the CST in the cerebral hemispheres is larger on the left, but no definite correlation of tract size with handedness has been demonstrated. Other studies have not revealed evidence of CST asymmetry.[33]

We find that asymmetries between MR parameters in the right and left CST are, on average, not significantly different from zero, and we uncover no evidence of a correlation between asymmetry and handedness. Across healthy volunteers, however, the range of asymmetries can range from large (fiber number and tract volume, which are more susceptible to variability in tract reconstruction than are the other MR imaging

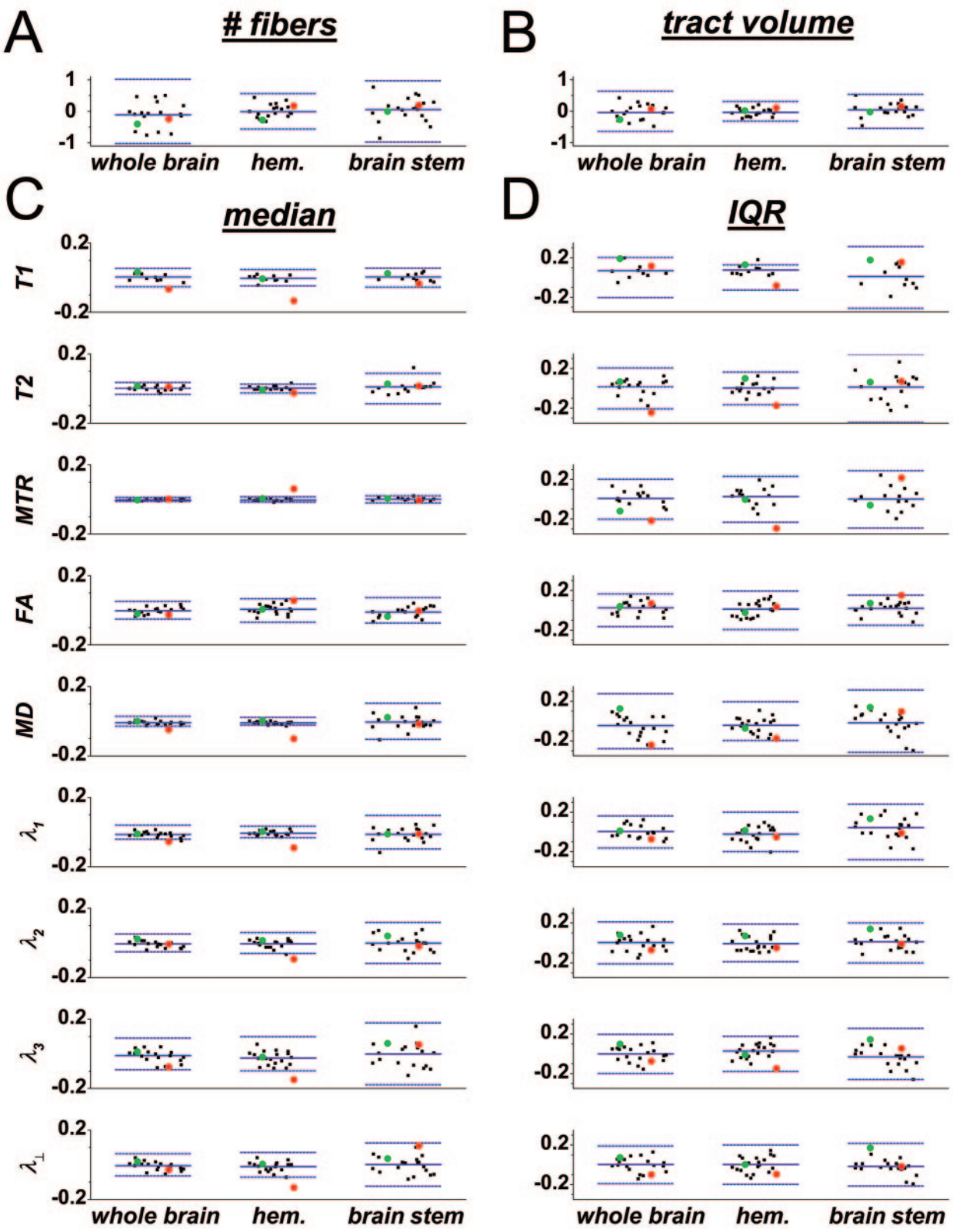

Fig 5. Asymmetry indices derived from reconstructed corticospinal tracts. (See the legend to Fig 4 for details on the presentation.) Vertical axis labels in *C* denote the MR imaging parameters for which asymmetry indices are shown; the same labels apply to panel *D*.

parameters) to quite small (eg, MTR). This range is illustrated in Figs 5 and 6. We also find (Fig 5 and Table 3) that asymmetries in the brain stem are generally larger than those in the hemispheres. This difference reflects greater variability of the MR imaging parameters within the brain stem, as seen in the second and third columns of Fig 3, and suggests that the CST in the brain stem might be better assessed in shorter segments than we used here.

Table 3: 99% normal ranges of absolute asymmetry indices for fiber number, tract volume, and summary statistics of MR parameters across our population of healthy volunteers

Reconstruction Type	No. of fibers	Vol.	T1	T2	MTR	FA	MD	λ_1	λ_2	λ_3	$\lambda_\perp$
No. of individuals	*20*	*20*	*11*	*17*	*15*	*20*	*20*	*20*	*20*	*20*	*20*
Whole brain	1.0	0.64	0.053 (0.20)	0.035 (0.21)	0.012 (0.20)	0.051 (0.16)	0.028 (0.28)	0.041 (0.16)	0.052 (0.21)	0.092 (0.20)	0.064 (0.19)
Hemispheres	0.56	0.31	0.047 (0.13)	0.026 (0.17)	0.015 (0.23)	0.068 (0.20)	0.023 (0.19)	0.033 (0.20)	0.059 (0.19)	0.098 (0.18)	0.071 (0.20)
Brain stem	0.97	0.54	0.054 (0.31)	0.087 (0.34)	0.021 (0.29)	0.073 (0.15)	0.10 (0.31)	0.097 (0.28)	0.12 (0.20)	0.18 (0.26)	0.13 (0.22)

Note:—MTR indicates magnetization transfer ratio; FA, fractional anisotropy; MD, mean diffusivity; $\lambda_\perp$, transverse diffusivity (average of λ_2 and λ_3). For the MR parameters, cutoffs for medians and interquartile ranges (in parentheses) are given. Data obtained at 3T.

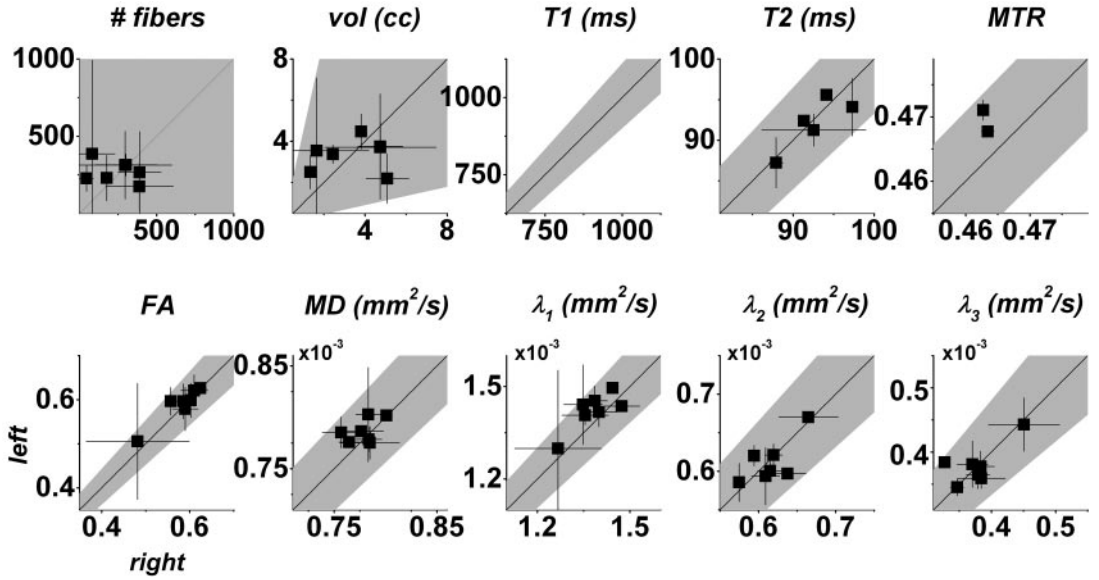

Fig 6. Scatterplots of fiber number, tract volume, and median MR imaging parameters across the whole-brain portions of the left versus right CSTs. Cross-scan means (squares) and 95% confidence intervals of the mean (error bars) are shown only for individuals who were scanned several times. In each plot, the 99% normal range derived from all healthy individuals (including those scanned only once) is shaded gray. Note that only the normal range is shown for T1 because we did not obtain absolute T1 data on multiple occasions from any individual.

Although only a subset of our subjects was scanned more than once, the results suggest that the finding of no average asymmetry across the population holds for individuals as well: in general, the average parameter asymmetry across scans of the same individual is not significantly different from zero. From the limited examples in our study, the major exception to this rule appears to be MTR, the reproducibility of which,[19] together with its sensitivity to neurologic disease and particularly MS,[34] makes it a very attractive parameter to study further.

Clinical Value of Our Approach. The parameters that we analyzed here were chosen because they are comparable across individuals and scans and because they are often abnormal in neurologic diseases. Several of the parameters were obtained directly from the DTI acquisitions, and others were obtained from other MR images that are coregistered with those acquisitions. Examining multiple non-DTI parameters along tracts reconstructed from DTI data represents an important novel contribution of our work. This approach has clinical utility because different MR imaging parameters might be sensitive to different aspects of pathology, and using a variety of them increases the chance that we will detect abnormalities in individuals with disease. Of course, in any situation in which multiple comparisons are made, we must take care to avoid assigning significance to detected abnormalities that are present by chance alone.

We show that the summary statistics derived from cross-individual distributions of MR imaging parameters, and their corresponding asymmetries, are, in general, well modeled by Gaussian distributions. The integrity of the CSTs in individuals with disease affecting those tracts can therefore be assessed quantitatively with the use of normal ranges derived from those Gaussian fits. Because these comparisons relate to a tract with a specific function (motor power), we hypothesize that abnormalities detected through this approach will relate specifically to neurologic dysfunction. Ongoing studies in our laboratory are evaluating the validity of this hypothesis in the case of MS.

We expect that the median MR parameters within tracts will ultimately be more clinically useful than the IQRs, if only because they are more straightforward to interpret. We present the IQRs in addition to the medians because they add a second level of sensitivity for detecting disease-related abnormalities. Abnormal IQRs are expected to be increased relative to those of healthy individuals because abnormalities in a tract tend to increase variability along that tract. An example of a tract-specific change that might preserve the median MR imaging parameters but alter the overall parameter distributions, and therefore increase the IQRs, would be several focal lesions with different properties along a single tract.

An alternative approach, in which the tracts are analyzed as

a function of location (eg, relative to specific anatomic structures), might be more sensitive than simple summary statistics such as median and IQR. This is suggested by our finding that the summary statistics are different in the hemispheric and brain stem portions of the CST and by the data in the middle and right columns of Fig 3, which demonstrate that parameter variation along a tract appears to be structured and not random. Such an approach would require careful cross-subject normalization and probably a larger data base of healthy controls.

Quantification of asymmetry is also important in the clinical setting. This is because the absolute value of the asymmetry index is likely to be increased in neurologic diseases that present asymmetrically, such as strokes, tumors, and demyelinating processes including MS. We expect that the use of asymmetry measurements in these conditions, together with measurement of the MR parameters themselves, will be useful for the quantitative assessment of response to therapeutic interventions in clinical trials.

Finally, although the tract-focused approach outlined here may potentially uncover abnormalities not detectable with a lesion-focused approach that relies on conventional T1- and T2-weighted imaging, clearly the 2 approaches are not completely distinct. For example, in the case of the individual with MS described here, the dominant cause of the absolute abnormalities and asymmetries in the CST-specific MR imaging parameters is likely the lesion itself, though there may be contributions from perilesional abnormalities along the CST.

Conclusion

We have demonstrated how fiber tracking with DTI can be used to estimate the distribution of MR imaging parameters within the right and left CSTs. The asymmetry between the 2 tracts tends to be small in healthy individuals and is not significantly different from zero across individuals. The 99% normal ranges for the individual MR imaging parameters and for the asymmetries derived from our collection of 20 healthy individuals can be used to detect tract-specific abnormalities in individuals with neurologic disease. Our results demonstrate the feasibility of combining fiber tracking with DTI with other MR images that cannot be used by themselves to isolate individual tracts.

Acknowledgments

We thank Terri Brawner, Karen DeBusk, Prachi Dubey, Jonathan Farrell, Eliza Gordon-Lipkin, Kathleen Kahl, Mathew Pulicken, and Setsu Wakana for their assistance with this project.

References

1. Mori S, Crain BJ, Chacko VP, et al. **Three-dimensional tracking of axonal projections in the brain by magnetic resonance imaging.** *Ann Neurol* 1999;45:265–69
2. Mori S, van Zijl PC. **Fiber tracking: principles and strategies—a technical review.** *NMR Biomed* 2002;15:468–80
3. Behrens TE, Woolrich MW, Jenkinson M, et al. **Characterization and propagation of uncertainty in diffusion-weighted MR imaging.** *Magn Reson Med* 2003;50:1077–88
4. Jones DK, Pierpaoli C. **Confidence mapping in diffusion tensor magnetic resonance imaging tractography using a bootstrap approach.** *Magn Reson Med* 2005;53:1143–49
5. Lazar M, Alexander AL. **Bootstrap white matter tractography (BOOT-TRAC).** *NeuroImage* 2005;24:524–32
6. Tournier JD, Calamante F, King MD, et al. **Limitations and requirements of diffusion-tensor fiber tracking: an assessment using simulations.** *Magn Reson Med* 2002;47:701–08
7. Bjartmar C, Trapp BD. **Axonal degeneration and progressive neurologic disability in multiple sclerosis.** *Neurotox Res* 2003;5:157–64
8. Block F, Dihne M, Loos M. **Inflammation in areas of remote changes following focal brain lesion.** *Prog Neurobiol* 2005;75:342–65
9. Simon JH, Kinkel RP, Jacobs L, et al. **A wallerian degeneration pattern in patients at risk for MS.** *Neurology* 2000;54:1155–60
10. Iannucci G, Tortorella C, Rovaris M, et al. **Prognostic value of MR and magnetization transfer imaging findings in patients with clinically isolated syndromes suggestive of multiple sclerosis at presentation.** *AJNR Am J Neuroradiol* 2000;21:1034–38
11. Vaithianathar L, Tench CR, Morgan PS, et al. **T1 relaxation time mapping of white matter tracts in multiple sclerosis defined by diffusion tensor imaging.** *J Neurol* 2002;249:1272–78
12. Jones DK, Horsfield MA, Simmons A. **Optimal strategies for measuring diffusion in anisotropic systems by magnetic resonance imaging.** *Magn Reson Med* 1999;42:515–25
13. Woods RP, Cherry SR, Mazziotta JC. **Rapid automated algorithm for aligning and reslicing PET images.** *J Comput Assist Tomogr* 1992;16:620–33
14. Basser PJ, Mattiello J, LeBihan D. **Estimation of the effective self-diffusion tensor from the NMR spin echo.** *J Magn Reson B* 1994;103:247–54
15. Basser PJ, Pierpaoli C. **Microstructural and physiological features of tissues elucidated by quantitative diffusion-tensor MRI.** *J Magn Reson B* 1996;111:209–19
16. Pajevic S, Pierpaoli C. **Color schemes to represent the orientation of anisotropic tissues from diffusion tensor data: application to white matter fiber tract mapping in the human brain.** *Magn Reson Med* 1999;42:526–40
17. Jiang H, van Zijl PC, Kim J, et al. **DtiStudio: resource program for diffusion tensor computation and fiber bundle tracking.** *Comput Methods Programs Biomed*. 2006;81:106–16
18. Bottomley PA, Ouwerkerk R. **The dual-angle method for fast, sensitive T1 measurement in vivo with low-angle adiabatic pulses.** *J Magn Reson B* 1994;104:159–67
19. Smith SA, Farrell JAD, Jones CK, et al. **Pulsed magnetization transfer imaging with body coil transmission at 3 Tesla: feasibility and application.** *Magn Reson Med* 2006;56:866–75
20. Lilliefors HW. **On the Kolmogorov-Smirnov test for normality with mean and variance unknown.** *J Am Stat Assoc* 1967;62:399–402
21. Tievsky AL, Ptak T, Farkas J. **Investigation of apparent diffusion coefficient and diffusion tensor anisotropy in acute and chronic multiple sclerosis lesions.** *AJNR Am J Neuroradiol* 1999;20:1491–99
22. Hiltunen J, Suortti T, Arvela S, et al. **Diffusion tensor imaging and tractography of distal peripheral nerves at 3 T.** *Clin Neurophysiol* 2005;116:2315–23
23. Alexander AL, Hasan KM, Lazar M, et al. **Analysis of partial volume effects in diffusion-tensor MRI.** *Magn Reson Med* 2001;45:770–80
24. Lazar M, Lee JH, Alexander AL. **Axial asymmetry of water diffusion in brain white matter.** *Magn Reson Med* 2005;54:860–67
25. Glenn OA, Henry RG, Berman JI, et al. **DTI-based three-dimensional tractography detects differences in the pyramidal tracts of infants and children with congenital hemiparesis.** *J Magn Reson Imaging* 2003;18:641–48
26. Parker GJ, Haroon HA, Wheeler-Kingshott CA. **A framework for a streamline-based probabilistic index of connectivity (PICo) using a structural interpretation of MRI diffusion measurements.** *J Magn Reson Imaging* 2003;18:242–54
27. Stieltjes B, Kaufmann WE, van Zijl PC, et al. **Diffusion tensor imaging and axonal tracking in the human brainstem.** *NeuroImage* 2001;14:723–35
28. Huang H, Zhang J, van Zijl PC, et al. **Analysis of noise effects on DTI-based tractography using the brute-force and multi-ROI approach.** *Magn Reson Med* 2004;52:559–65
29. Kertesz A, Geschwind N. **Patterns of pyramidal decussation and their relationship to handedness.** *Arch Neurol* 1971;24:326–32
30. Nagae-Poetscher LM, Jiang H, Wakana S, et al. **High-resolution diffusion tensor imaging of the brain stem at 3 T.** *AJNR Am J Neuroradiol* 2004;25:1325–30
31. Fabiano AJ, Horsfield MA, Bakshi R. **Interhemispheric asymmetry of brain diffusivity in normal individuals: a diffusion-weighted MR imaging study.** *AJNR Am J Neuroradiol* 2005;26:1089–94
32. Rademacher J, Burgel U, Geyer S, et al. **Variability and asymmetry in the human precentral motor system: a cytoarchitectonic and myeloarchitectonic brain mapping study.** *Brain* 2001;124:2232–58
33. White LE, Andrews TJ, Hulette C, et al. **Structure of the human sensorimotor system. II. Lateral symmetry.** *Cereb Cortex* 1997;7:31–47
34. Schmierer K, Scaravilli F, Altmann DR, et al. **Magnetization transfer ratio and myelin in postmortem multiple sclerosis brain.** *Ann Neurol* 2004;56:407–15